Journal of Geochemical Exploration 161 (2016) 49–61

Contents lists available at ScienceDirect

Journal of Geochemical Exploration

journal homepage: www.elsevier.com/locate/jgeoexp

The discovery of the metallic particles of groundwater from the Dongshengmiao polymetallic deposit, Inner Mongolia, and their prospecting significance

Yingkui Li [a], Jianjin Cao [a,b,*], Philip K. Hopke [c], Robert F. Holub [c], Tao Jiang [a]

[a] School of Earth Science and Geological Engineering, Sun Yat-sen University, 510275, PR China
[b] Geological Process and Mineral Resources Exploration of the Key Laboratories, Guangdong Province, 510275, PR China
[c] Center for Air Resources Engineering and Science Clarkson University, NY 13699, USA

ARTICLE INFO

Article history:
Received 2 April 2015
Revised 29 September 2015
Accepted 20 October 2015
Available online 21 October 2015

Keywords:
Dongshengmiao polymetallic deposit
Groundwater
Particles
Prospecting

ABSTRACT

In recent years, new methods for seeking concealed ore bodies have become an active area of ore prospecting. Previous studies of water geochemistry have usually been confined to the analysis of the elemental content of surface water, and performing metallogenic predictions based on high element contents. This paper represents the first use of transmission electron microscopy (TEM) to study particles of groundwater in or around the ore district. Comparing the results of the TEM characterization of well waters near the ore district with those of groundwater samples from the deep ore district (hereinafter referred to as the concept of "deep groundwater"), the particles found in both types of water samples were similar. The ore-forming metal particles, such as Fe, Cu, Pb and Zn-bearing particles, are found in both well water and deep groundwater, while the samples in the well waters of the background area (hereinafter referred to as the concept of "background water") mainly contain only particles, such as $CaCO_3$, $Ca(OH)_2$, silicate, oxide of Na, K and Fe. In addition, the composition and characteristics of particles from well waters and deep groundwater revealed that they are derived from the concealed ore bodies. Faulting and oxidation are the main mechanisms of particle formation. Because well water samples are similar to the deep groundwater samples, they can be conveniently collected at ground level, and may be used to predict the presence of a deep ore resource. This research establishes a new method for geochemical prospecting using groundwater particles. These particles can reflect more abundant and accurate information regarding the concealed ore bodies than the content of elements. The discovery of metal containing particles in groundwater may improve water-based geochemical prospecting method.

1. Introduction

With the rapid growth of the demand for mineral resources, production requirements cannot be fully met by mining surface or shallow surface deposits. Thus, methods to find concealed ore bodies are important in ore prospecting. Concealed deposits are generally buried in deep positions that may only exhibit weak mineralization information on the earth's surface. To accurately obtain information on deep ore bodies, exploration using new approaches that find concealed deposits is required.

Currently, geophysical and geochemical methods are the common approaches of ore exploration (Wang et al., 2013; Varentsov et al., 2013; Kelley et al., 2003). To study the regional gravity and magnetic anomaly data, geophysical methods are able to delineate the abnormal area. For example, by using the controlled source audio-frequency magneto-telluric (CSAMT) and spectral induced polarization method (SIP), Song et al. (2012) found an obvious anomaly in the fracture alteration zone of the Sanshandong-Jiaojia area, eastern Shandong Province. In addition, a deep gold mine was delineated on the basis of these findings. Varentsov and Sokolova (2003) used telluric electromagnetic sounding (MT) and the 3-D model to study massive sulfide deposits.

Geochemical methods are mainly based on the dispersive and centralized rule of elements, that is, ore can be found by identifying an anomalous elemental behavior. Common geochemical methods include: electrogeochemical method (Antropova et al., 1992; Ryss and Goldberg, 1973), Enzyme leach (Clark et al., 1990), mobile metal ions (Wang et al., 1997; Mann et al., 1998), soil secondary halo method (Cameron et al., 2004; Kelley et al., 2003), biogeochemical methods (Cole, 1971; Arne et al., 1999; Hill and Hill, 2003), geogas methods (Wang et al., 1997, 1999; Tong et al., 1998; Arne et al., 1999; Wang, 2003; Johanna et al., 2011; Cao et al., 2009, 2010a,b, 2015; Wei et al., 2013; Ye et al., 2014; Hu et al., 2015), and hydrogeochemical method (Mohammadzadeh and Chary, 2005; Taufen, 1997; Shvartsev, 2009; Cameron et al., 2004).

In particular, the hydrochemical prospecting method is one in which groundwater or surface water samples are collected for geochemical analysis. The method can be effective in the exploration of mineral

* Corresponding author at: School of Earth Science and Geological Engineering, Sun Yat-sen University, 510275, PR China.
E-mail address: eescjj@mail.sysu.edu.cn (J. Cao).

http://dx.doi.org/10.1016/j.gexplo.2015.10.013
0375-6742/

resources based on the anomalous element content of the collected water. Early groundwater geochemistry is mainly used in radioactive hydrochemical prospecting, which is generally used for uranium exploration (Nikic et al., 2008; Rani et al., 2013). For example, Singha et al. (2003) collected water samples in some areas of Himachal and Punjab, India, and then used the fission track and laser fluorometric techniques to analyze the content of uranium in water. Rani et al. (2013) used inductively couple plasma-mass spectrometry (ICP-MS) to determine the concentrations of radioactive elements in drinking water collected in northern Rajasthan.

With the development of analytical processing technology, research objectives have gradually extended to seeking deposits of heavy metal, copper, sulfide and gold (McHugh, 1988; Cidu et al., 1995; Eppinger et al., 2012). For example, Miller et al. (1982) performed an analysis on water samples from two porphyry copper deposits in Midwestern Puerto Rico, and the experimental results indicated that the water dispersion halo could be used to predict a deposit under certain geochemical conditions. Based on the relative solubility of ore elements, Huff (1948) used a semi-quantitative dithizone colorimetric method to analyze the content of heavy metal element in water samples.

The analytical methods generally used in hydrochemical prospecting, include the determination of the water element concentrations, pH value, and ionic concentrations (Lakshmanan et al., 2003; Kumar et al., 2006). Water can be identified based on its abnormal elemental content. However, a relatively high elemental content can be caused by many factors, such as the presence of carbonaceous shale, lithology, topographic relief, karst fracture zone and so on (Erg, 2005). These factors may not necessarily represent a relationship with a concealed ore body. In addition, different sampling and processing methods such as using the mesh filter for sample preparation may cause the loss of some unstable elements. Some elements will be removed due to the use of different meshes, which may affect the accuracy of the test results.

In this paper, the selected study area is the Dongshengmiao polymetallic deposit in the Wulatehou Banner in the Bayannaoer League, Inner Mongolia, which is an important polymetallic sulfur production area in China. To find deeply buried or covered mineral resources, groundwater samples were collected in or near the ore district, and the particles separated from the groundwater were observed using transmission electron microscopy (TEM). This study represents the first time that nanoparticles or nearly nano-scale particles of metal-bearing materials suspended in groundwater have been studied. The results of this study may provide the foundation for establishing a new, multidisciplinary method for the geochemical prospecting of groundwater particles.

2. Geological setting

The Dongshengmiao polymetallic deposit is a large-scale deposit in the Wulatehou Banner in the Bayannaoer League, Inner Mongolia, and the mining area is located in the border area between the middle of Langshan Mountain and the Hetao plain (Fig. 1). The area of the mining region is nearly 4.65 km^2.

From old strata to new strata, the distributions of regional stratigraphic succession are as follow: the Lower Proterozoic Wulashan group (Pt_1wn), the Mesoproterozoic Langshan group (Pt_2ls), the Upper Paleozoic Carboniferous–Permian (C–P), the Mesozoic Shiguai group of Jurassic system ($J_{1\text{-}2}sh$) and Lisangou group of Cretaceous system (K_1L^2), the Cenozoic Tertiary system (R) and Quaternary system (Q). The strata exposed in the mining area are incomplete, and the mainly exposed strata in the ore district are the Mesoproterozoic Langshan group (Pt_2ls), the Mesozoic strata (K) and the Cenozoic strata (Q). The Paleozoic strata are missing (Jiang, 1993; Liu and Qian, 2012). The main ore-bearing rock series is in the Mesoproterozoic Langshan group, with the polymetallic sulfide deposit hosted in the middle-upper transgression strata. The Mesozoic strata are distributed mainly in the northern part of the ore district, where only the Lower Cretaceous Lisangou Formation is exposed. The Lisangou group overlaps the Langshan group, which is the main cap rock of this area. The lithology of this group is dominated by amaranthine gravel containing clay rock, which is intercalated with thin glutenite. The Cenozoic erathem in this area include Tertiary and Quaternary systems. The former is composed of glutenite, with a few conglomerates. The latter mainly contains loose alluvium, diluvium, saprolite and slope wash, which is generally composed of gravel and sand clay (Liu and Qian, 2012; Chen and Peng, 2008). The main geological structure in the mining area are faulting and folding. The Langshan Mountain-front fault passes

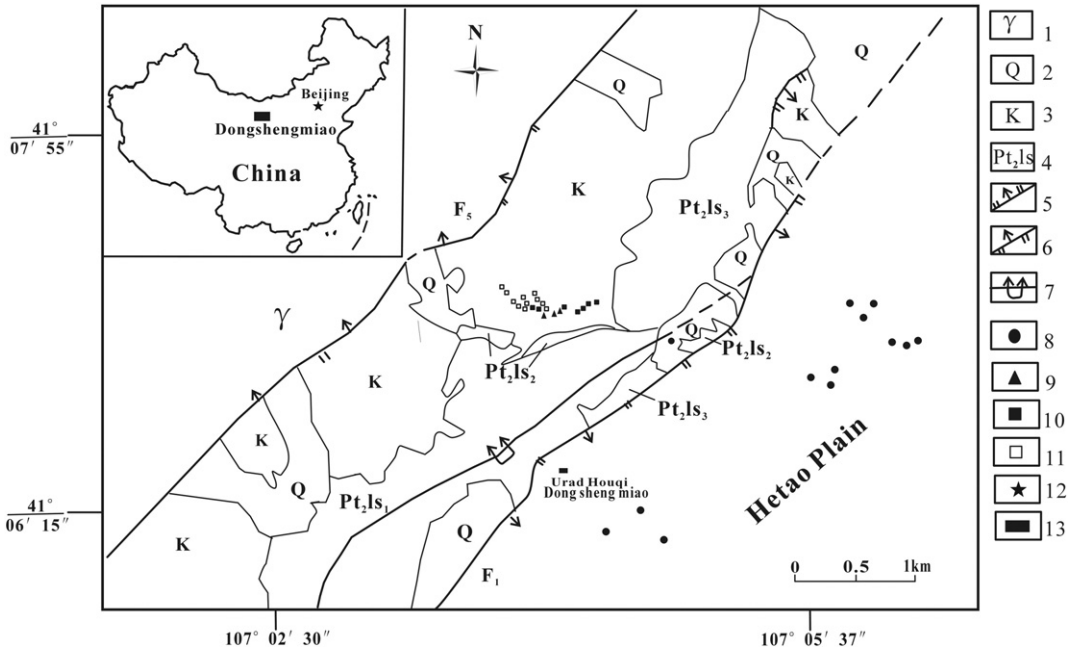

Fig. 1. Sampling locations and schematic geological map of Dongshengmiao ore district, Inner Mongolia. 1. Granite; 2. Quaternary; 3. Cretaceous red beds; 4. rock section of Mesoproterozoic Langshan group; 5. normal fault; 6. reverse fault; 7. overturned anticline; 8. well water sampling points; 9. deep groundwater sampling points (sampling depth: 400–449 m); 10. deep groundwater sampling points (sampling depth: 450–499 m); 11. deep groundwater sampling points (sampling depth: 500–550 m); 12. the capital of China; 13. the study area (redrawn according to profile map provided by Chen and Peng, 2008). Inset shows the location of this study area in China.

through the deposit. The mining area spreads along the northeast to southwest, between F1 and F5, which are two regional faults (Fig. 1). The general structure of the ore district is an asymmetric compound synclina fold, which exhibits the form of lifting to the west and falling to the east (Chen and Peng, 2008).

The ore bodies in this mining area are located at nearly 200–550 m under the surface. And the ore minerals are mainly primary minerals, which mainly contain metallic minerals such as pyrite, pyrrhotite, sphalerite, galena, chalcopyrite, and binarite. Using underground mining, the mine in the Dongshengmiao ore district is still at mining stage, and the mineral resources are abundant. The main economic mine in this area is pyrites, reserves of zinc, lead and copper also reach large or medium scale. Examples of useful components in the minerals are distributed as follows: zinc is mainly present in sphalerite, pyrrhotite, and pyrite; lead primarily comes from galena; copper mainly occurs in chalcopyrite; and silver fills in the fissures of sphalerite, galena and chalcopyrite in the form of native silver or fills in the fissure of pyrite in the form of kustelite (Peng et al., 2007; Liu and Qian, 2012; Jiang, 1993). Because of late regional metamorphism, this deposit is considered to be a set of sedimentary formations that contain carbonaceous silty mudstone and carbonate intercalated with submarine volcanic material.

3. Sampling and analysis methods

The collected groundwater samples can be divided into three types: deep groundwater, well water and background water. The pH values exhibit minor differences in these samples, approximately 7.8 on average, with a range of 7.5 to 8.1.

The numbers of deep groundwater, well water and background water samples were respectively 21, 13 and 7. The locations of the sampling sites are shown in Fig. 1. The specific sampling method was performed as follows: 500 ml wide-mouthed polyethylene bottles were used to collect the water. The deep groundwater samples were collected in the deep mining roadway of the Dongshengmiao deposit. The bottles were used to collect the deep groundwater that seeped from the fissure, and the sampling depth was close to the depth of concealed ore bodies, which was nearly 400 m, 450 m, 500 m or 550 m under the surface. The bottles were placed below the fissure water-developed zone and recovered when approximately 300 to 400 ml of water samples had been collected. Well waters were collected in two locations, one location was in the irrigation wells southwest of the mine, and the depth of wells was nearly 20 m or 30 m. The other location was in the wells southeast of the mine, and the depth of those wells was about 50 m or 100 m. The background waters were collected in the motor-pumped wells in Tianjitai town, southwest of Wuyuan County, which is nearly 90 km away from the Dongshengmiao mining area. These sampling sites are unaffected by the mining area and the sampling depth was either 12 m or 60 m. The final step was to assign a sample number and store the samples at room temperature. The polyethylene bottles had been washed with high purity water and dried before use. The preservation temperature of the samples is around 25 to 27 °C.

Table 1
The EDS data of particles (ID: 1–13).

Element	Nano-particle number												
	1	2	3	4	5	6	7	8	9	10	11	12	13
Weight O%	34.56	29.23	8.99	39.59	31.43	10.08	35.79	29.9	6.29	5.39	7.44	32.65	39.48
Atomic O%	46.49	56.58	28.6	59.16	55.47	25.33	59.43	51.96	32.55	28.38	42.61	62.39	67.56
Weight Si%	2.55				0.42		0.01	4.13		0.13			0.22
Atomic Si%	1.95				0.42		0.01	4.09		0.39			0.21
Weight Al%				19.48				2.41					0.09
Atomic Al%				17.26				2.48					0.09
Weight Fe%	38.8	62.95	2.79	0.83	13.06	11.88		0.7		0.91	12.23	64.37	47.17
Atomic Fe%	14.95	34.9	2.54	0.35	6.6	8.55		0.35		1.38	20.06	35.23	23.12
Weight Ca%	2.94		2.06		0.83	11.26	1.51	4.77					3.57
Atomic Ca%	1.58		2.62		0.58	11.29	1	3.31					2.43
Weight Na%	0.73				8.53	1.36	7.5	14.57					1.61
Atomic Na%	0.06				10.47	2.38	8.67	17.62					1.92
Weight K%						3.96	0.38	1.78				0.84	
Atomic K%						4.07	0.33	1.26				0.65	
Weight Mg%	0.34	4.01				0.02	0	1.15				0.71	1.36
Atomic Mg%	0.3	5.12				0.03	0	1.31				0.9	1.53
Weight S%	0.38	0.91			0.39	3.45	0.75	1.61					
Atomic S%	0.25	0.88			0.34	4.33	0.62	1.4					
Weight F%				9.17	4.62		5.69						
Atomic F%				11.54	6.87		7.96						
Weight Cl%	1.22	2.87				9.32	0.73	1.73					
Atomic Cl%	0.74	2.51				10.57	0.55	1.35					
Weight I%									38.19	27.32			
Atomic I%									24.89	18.13			
Weight Mn%				0.63	19.77	28.12	27.22	1.04				0.77	4.86
Atomic Mn%				0.27	10.16	20.58	13.16	0.53				0.43	2.42
Weight Pb%								3.73					
Atomic Pb%								0.5					
Weight Zn%					20.91	17.27	20.49	32.42					1.6
Atomic Zn%					9.03	10.62	8.32	13.78					0.67
Weight Cu%			76.58	30.28									
Atomic Cu%			61.34	11.39									
Weight Au%											80.31		
Atomic Au%											37.32		
Weight Ag%									55.5	66.23			
Atomic Ag%									42.55	51.7			
Weight Co%			1.77			3.22							
Atomic Co%			1.52			2.2							
Weight Sn%			7.78										
Atomic Sn%			3.34										

Table 2
The EDS data of particles (ID: 14–25).

Element	Nano-particle number											
	14	15	16	17	18	19	20	21	22	23	24	25
Weight O%	9.49	10.01	18.57	21.82	17.63	4.63	15.88	51.29	43.82	71.41	59.83	48.82
Atomic O%	26.49	28.4	46.99	47.58	38	24.01	40.23	72.06	65.63	81.43	72.93	74.48
Weight Si%		0.02		0.2						15.35	0.72	1.42
Atomic Si%		0.03		0.25						9.97	0.5	1.23
Weight Al%		6.6	0.32	0.13	0.31					3.91		
Atomic Al%		11.11	0.48	0.17	0.39					2.64		
Weight Fe%	58.28	1.49	3.48	1.1	1.03	1.27				1.37		29.85
Atomic Fe%	46.57	1.21	2.52	0.68	0.63	1.89				0.44		13.04
Weight Ca%		0.86	1.43	1.85			0.56	43.67	53.44	0.83		3.74
Atomic Ca%		0.98	1.44	1.61			0.57	24.49	31.94	0.37		2.28
Weight Na%				4.76	18.52	3.39	5.49	1.01	2.09	2.88	19.75	1.52
Atomic Na%				7.23	27.77	12.23	9.69	0.98	2.06	2.28	16.67	1.61
Weight K%						3.69	4.24		0.42	0.22	13.78	
Atomic K%						7.83	4.4		0.26	0.1	6.87	
Weight Mg%		0.2		0.69				1	2.09	3.21		1.02
Atomic Mg%		0.38		0.99				0.93	2.06	2.41		1.02
Weight S%				8.65			3.72				1.46	
Atomic S%				9.41			4.71				0.88	
Weight Cl%		0.14		0.45	0.47	9.12	7.85			0.27	2.57	1.05
Atomic Cl%		0.19		0.44	0.46	21.32	8.98			0.14	1.41	0.72
Weight Mn%	15.6									0.14		12.54
Atomic Mn%	12.67									0.04		5.57
Weight Pb%						76.27	17.47					
Atomic Pb%						30.48	3.41					
Weight Zn%				31.68	61.56		31.45			0.21	1.42	
Atomic Zn%				16.9	32.45		19.49			0.05	0.42	
Weight Cu%		79.54	76.19	25.69			13.29					
Atomic Cu%		56.82	48.54	14.1			8.47					
Weight Co%		1.09			0.44	1.58						
Atomic Co%		0.84			0.26	2.22						
Weight Cr%	16.61								0.2			
Atomic Cr%	14.25								0.09			

Particles in the collected groundwater samples were analyzed using transmission electron microscopy (TEM, Tecnai G2F30S-Twin, America) analysis and energy dispersive X-ray analysis (EDX, America) at the testing center of Yangzhou University. The specific parameters of the test instruments were as follows: the maximum accelerating voltage was 300 kV, the dot resolution was 0.20 nm, the linear resolution was 0.102 nm, the resolution of HR STEM was 0.17 nm, and the maximum magnification of the TEM and STEM was one million times and three million times. Samples were pre-processed to ensure that the nickel screens were in good condition before the TEM analysis. To avoid contamination, sample pretreatment process was performed under the condition of a clean bench. To process each sample, the bottles were shaken gently to reduce the impact of the uneven distribution of particles caused by gravitational settling. To deposit the particles on the mesh, the samples were dropped onto the nickel screen using a pipette. The sample number was then assigned to the nickel screen. This deposition step was repeated four to five times, followed by air-drying of the sample. To prevent damaging the grid, tweezers were used to fix the nickel screen to the sides of the nets. The ready-made nickel screen was then placed into a clean sample box when the water samples had completely evaporated. To avoid cross contamination from the prior sample, the pipette tip was changed before preparing the next sample.

The microscopic analysis mainly recorded the X-ray spectral analysis of the elements in each particle, providing the atomic percentage of each of the observed elements, TEM images, selected area electron diffraction (SAED) patterns and high resolution transmission electron micrographs (HRTEM). From these experimental data, the elements and crystal structure were determined to enable the estimation of the probable mineral composition from the elemental ratios. Because the grid material contains carbon and nickel, these two elements were eliminated in the analysis.

4. Experimental data

More than 80 particles and 60 particles were detected in the deep groundwater and well water samples, and the majority of them were ore-forming particles, such as Fe, Cu, Pb, Zn-bearing particles. Hg, Bi,

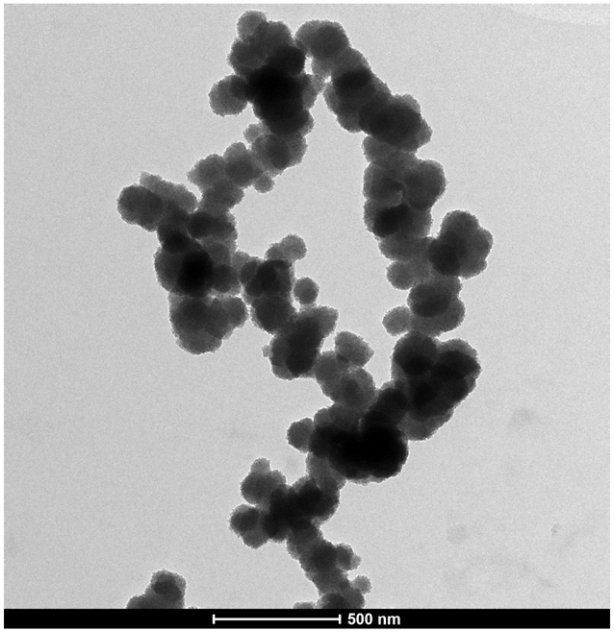

Fig. 2. TEM image of Fe-bearing hydroxide particles.

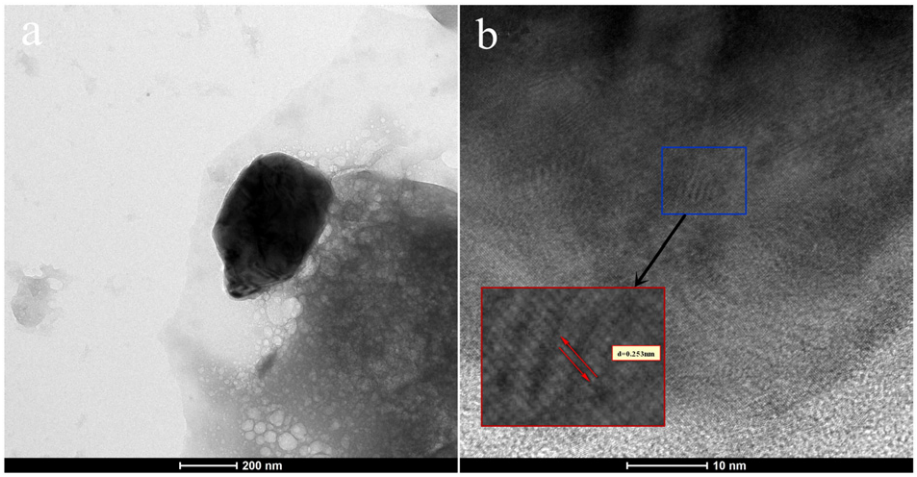

Fig. 3. Hematite particle: a. TEM image, b. HRTEM image.

Ti, Cr, Mo, W, Sn, Ba-bearing particles and some common elements (such as Si, Al, Ca, Na, K and Mg) were also present in both the deep groundwater and well water samples, but these were of little help for exploration, and the focus was placed on the combination and components of ore-forming particles. More than 10 particles were examined in the background water, and the particles were mainly $CaCO_3$, $Ca(OH)_2$, oxides of Si, Na, K and Fe. The EDS data are shown in Tables 1 and 2.

4.1. Particles of deep groundwater samples

The TEM analysis of deep groundwater indicated that the samples contained a variety of metal-bearing particles. A catenulate assemblage of Fe-bearing particles (ID: 1) is shown in Fig. 2. The EDS analysis shows that the main components of the assemblage are Fe (38.8%) and O (34.6%), with minor amounts of Ca (2.9%), Si (2.6%) and Cl (1.2%). The O to Fe atomic ratio of the assemblage is 3.11 (46.5/15.0), suggesting that it may be iron hydroxides. A nearly rectangular Fe-bearing particle (ID: 2) is shown in Fig. 3.a. The main component of the particle is Fe (63.0%) and O (29.2%), and the O to Fe atomic ratio is approximately 3/2(56.6/34.9). The interplanar spacing is 0.253 nm (Fig. 3.b), suggesting that the particle is hematite (Randrianantoandro et al., 2001; Costantini et al., 2006).

Fig. 4 shows an irregular Cu-bearing particle (ID: 3). The main composition of the particles a: Cu (76.6%), O (9.0%) and Sn (7.8%). The EDS data suggests that the particles are mainly Cu and Cu_2O, with minor amounts of SnO_2. Cu-bearing particles with dark color are shown in the upper right portion of Fig. 5. These particles are mainly composed of Cu (30.3%), O (40.0%) and Al (19.5%); as a result, these particles may be oxides of Cu and Al.

An elliptical Zn and Mn-bearing particle (ID: 5) is shown in the middle of Fig. 6. The color of the nanoparticle is dark, and its size is approximately 400 nm × 500 nm. It is mainly composed of Zn (20.9%), Mn (19.8%) and O (31.4%). The atomic percentages suggest oxides of Zn and Mn. An irregular assemblage of Zn and Mn-bearing particles (ID: 6) are shown in Fig. 7, with its main components being Zn (17.3%), Mn (28.1%) and Fe (11.9%). The atomic percentages suggest that these particles may be oxides of Zn, Mn and Fe. The irregular shapes of the Zn and Mn oxide particles (ID: 7) in Fig. 8 suggest aggregates because the edges of a single particle are uncertain. The main component of

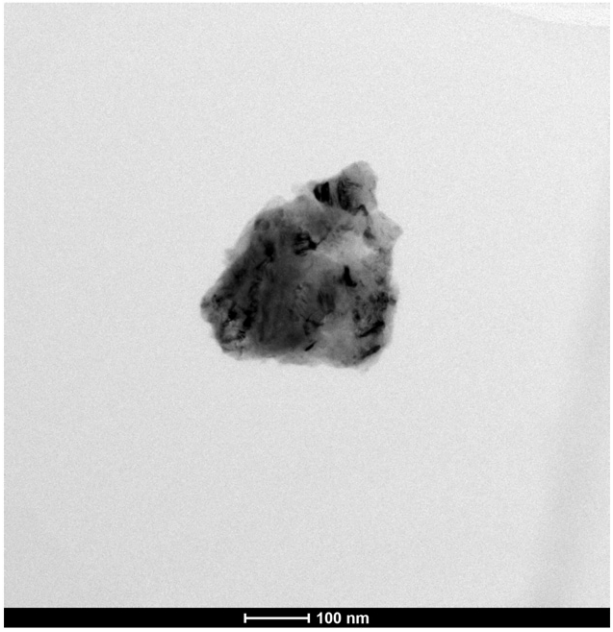

Fig. 4. TEM image of Cu-bearing particle.

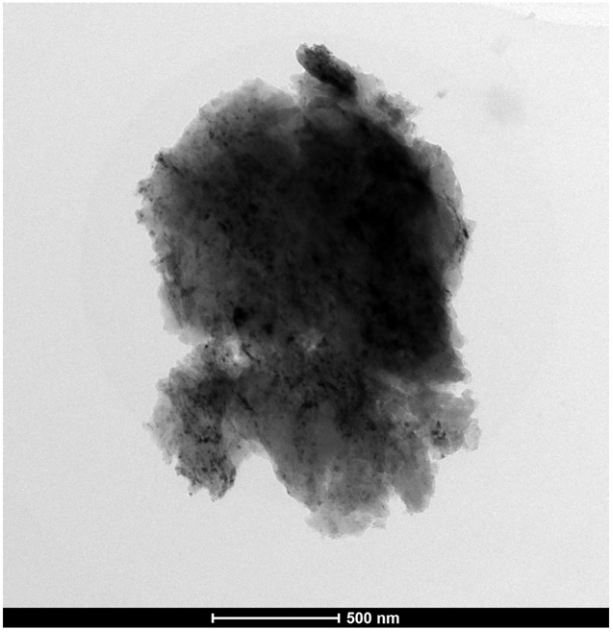

Fig. 5. TEM image of Cu, Al oxide particles.

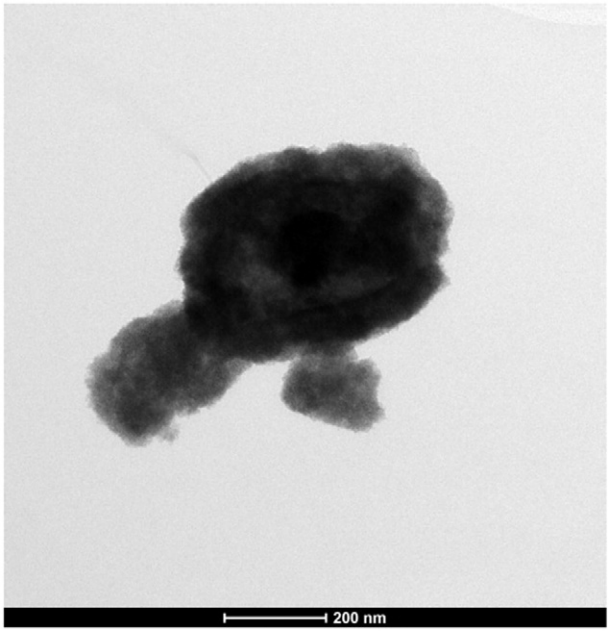

Fig. 6. TEM image of Zn, Mn oxide particle.

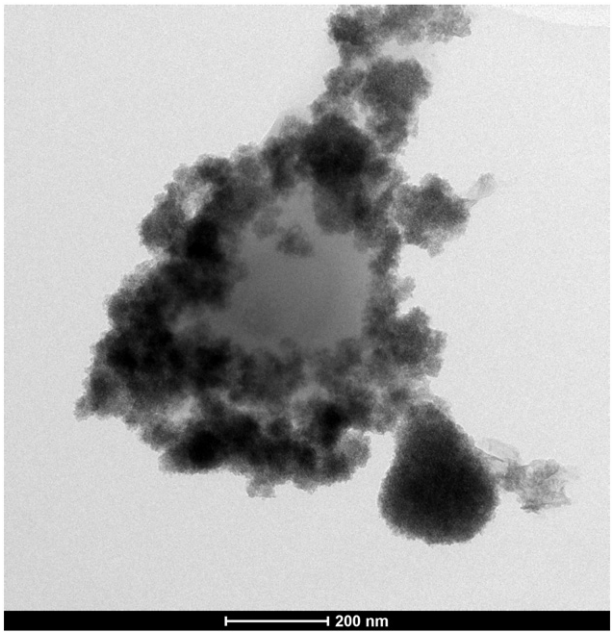

Fig. 8. TEM image of Zn, Mn oxide particles.

these particles is Zn (20.5%), Mn (27.2%) and O (35.8%), with minor amounts of Na (7.5%) and Ca (1.5%). The elemental atomic compositions reveal that Zn is 8.3%, Mn is 13.2% and O is 59.4%, which suggests that the particle is Zn and Mn oxide.

Under TEM analysis, a few Pb-bearing particles were observed. Fig. 9 shows a spherical Zn, Pb-bearing particle (ID: 8) that is 400 nm in diameter. The EDS analysis reveals that its main components are Zn (32.4%), Pb (3.7%) and O (29.9%), with a minor amount of S (1.6%).

Figs. 10 and 11 show spherical aggregations of Ag-bearing particles, with their diameter ranging from 50 nm to 150 nm. The EDS analysis indicates that the particles (ID: 9) in Fig. 10.a mainly contain Ag (55.5%) and I (38.2%). The HRTEM image (Fig. 10.b) indicates that the particle is crystalline in two directions, with an approximately 60° angle. By measuring the interplanar spacing, the distance is determined to be approximately 0.373 nm. The particles (ID: 10) in Fig. 11.a mainly contain Ag (66.2%) and I (27.3%), with a minor amount of Fe (0.9%). By analyzing the HRTEM image in Fig. 11.b, the features are found to be the same as those in Fig. 10.b. The distance between the two crystal faces is 0.363 nm. The atomic percentages suggest that the particles are mainly AgI and Ag.

Natural gold particles (ID: 11) were also found via TEM analysis. A spherical Au-bearing particle is shown in the lower-left corner of Fig. 12. The particle is dark in color, with a diameter of approximately 40 nm. The EDS analysis reveals that their main components are Au (80.3%), with minor amount of Fe (12.2%) and O (7.4%). Based on the atomic percentage, there is mostly Au with iron oxides in the particle.

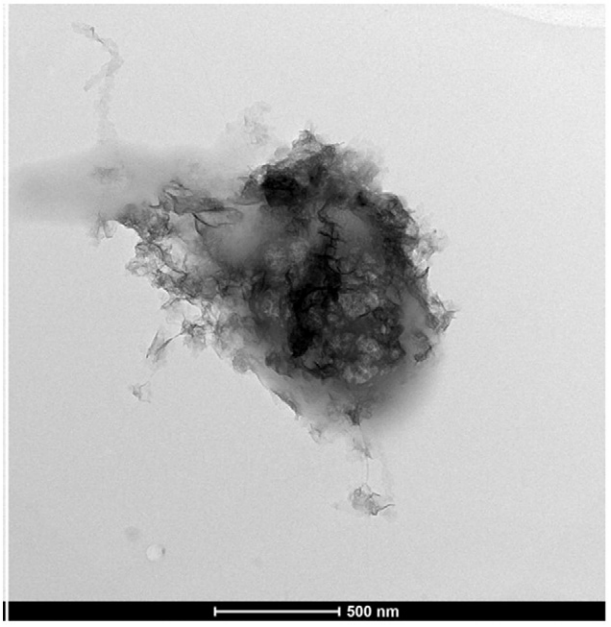

Fig. 7. TEM image of Zn, Mn, Fe oxide particles.

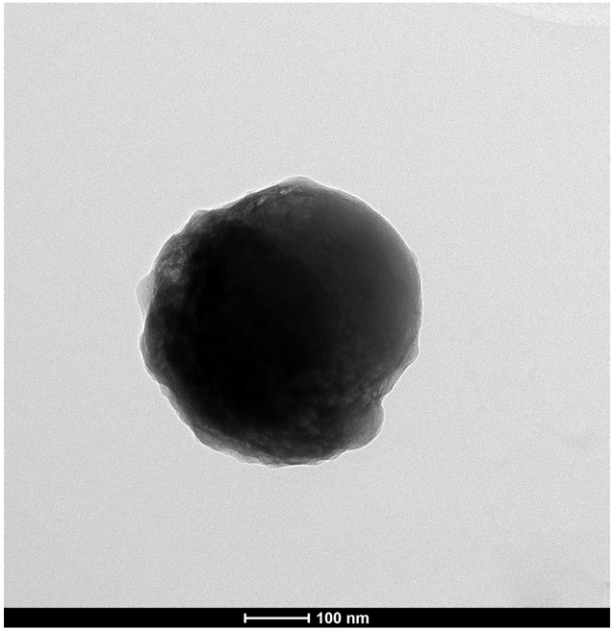

Fig. 9. TEM image of Zn, Pb-bearing particle.

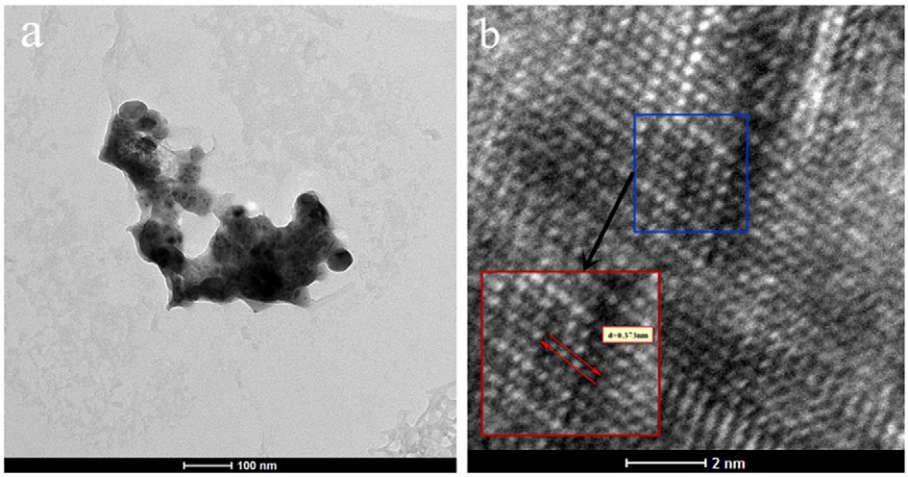

Fig. 10. AgI particle: a.TEM image, b. HRTEM image.

4.2. Particles of well water samples

Fe-bearing particles were the most common ones that exist in well water. These particles exist in the form of oxides and hydroxides. A spherical particle (ID: 12) with 276 nm in diameter was observed in Fig. 13.a. It was mainly composed of Fe (64.4%) and O (32.7%). The SAED pattern in Fig. 13.b revealed that this particle was single crystal. The interplanar spacing was 0.297 nm (Fig. 13.c), which indicated it was magnetite. Fig. 14 showed a nearly spherical particle (ID: 13) with 467 nm in diameter, it contained high amounts of Fe (47.2%) and O (39.5%), and a small amount of Mn (4.86%) and Zn (1.60%). According to the EDS analysis, the atomic percentage ratio of Fe/O was about 1/3 (23.1/67.6), suggesting it was iron hydroxide, with a minor amount of MnO_2. The experiments showed that Fe, Mn and Cr usually appeared together. Fig. 15 showed irregular particles (ID: 14) with dark color, and their component were Fe (58.3%), Mn (15.6%), Cr (16.6%) and O (9.5%), suggesting they were oxides of Fe, Mn and Cr.

The aggregation of Cu-bearing particles (ID: 15) was observed in Fig. 16.a. The main component of these particles was Cu (79.5%) and O (10.0%). According to the HRTEM image (Fig. 16.b), the interplanar spacing was 0.182 nm. The atomic percentage ratio of Cu/O was closely 2/1 (56.8/28.4), which may indicate that it was Cu_2O. Irregular Cu-bearing particles (ID: 16) with rough edges are shown in Fig. 17. The EDS data revealed that it had a high content of Cu (76.2%) and a low content of O (18.6%), and the atomic percentage ratio of Cu/O was close to 1 (48.5/47.0), suggesting it was CuO.

Fig. 18 showed aggregation of Zn, Cu-bearing particles (ID: 17) with dark color. They were mainly composed of Zn (31.7%), Cu (25.7%) and O (21.8%). Combined with the EDS analysis data, it would indicate that these particles were mainly oxides of Zn, Cu. A nearly spherical Zn-bearing particle (ID: 18) 517 nm in diameter was observed in Fig. 19. It was mainly composed of Zn (61.6%), with a minor amount of O (17.6%) and Na (27.8%). According to the atomic percentage, Zn/O is close to 1, suggesting it could be ZnO.

Irregular Pb-bearing particles (ID: 19) with dark color were observed in Fig. 20. The EDS analysis data revealed that these particles had a high content of Pb (76.3%), with a minor amount of O (4.6%), Fe (1.3%) and Co (1.6%). And the atomic percentages of Pb and O were respectively 30.5% and 24.0%, suggesting it was oxide of Pb. Fig. 21 showed multi-metal particles (ID: 20). The main component of these particles was Zn (31.5%), Cu (13.3%) and Pb (17.5%). According to the atomic percentage, it could be oxide of Zn, Pb and Cu.

4.3. Particles of background water samples

Fig. 22 showed a relatively regular Ca-bearing particle (ID: 21), and its size was 580 nm × 880 nm. According to the EDS data, it was mainly composed of Ca (43.7%) and O (51.3%). The atomic percentage ratio of Ca/O is about 1/3 (24.5/72.1), which indicated it was $CaCO_3$. A hexagonal Ca-bearing particle (ID: 22) was observed in Fig. 23. Its main contents were Ca (53.4%) and O (43.8%), with a little Mg (2.1%). Based on

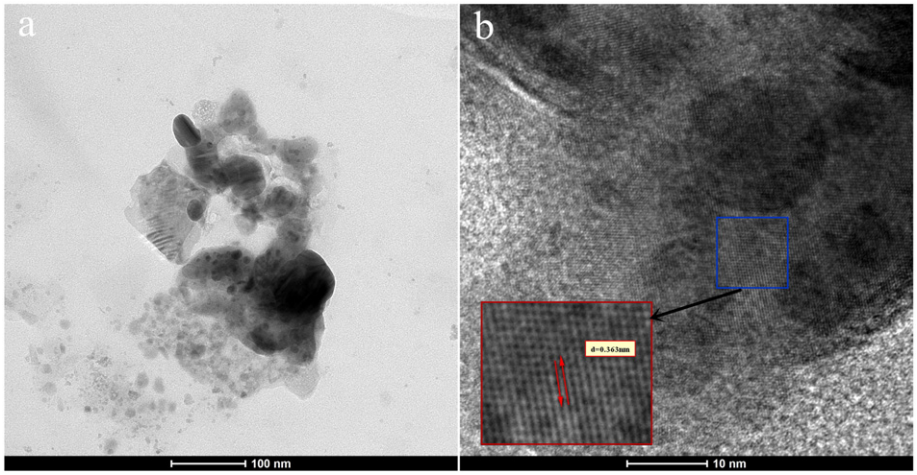

Fig. 11. AgI, Ag particle: a.TEM image, b. HRTEM image.

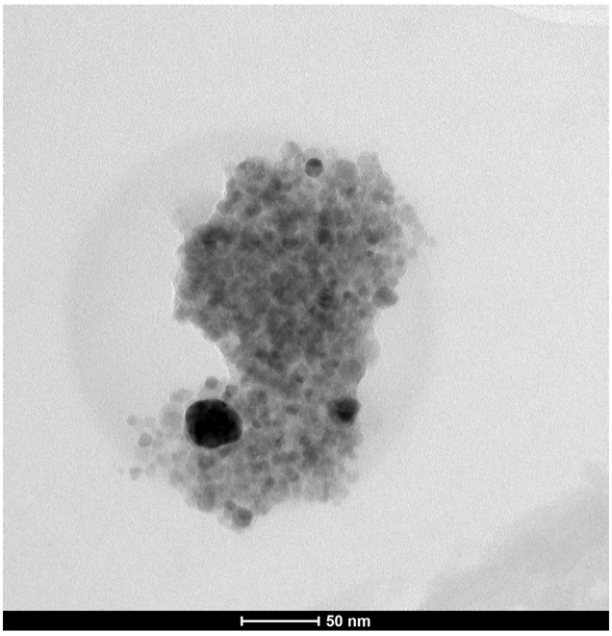

Fig. 12. TEM image of Au-bearing particle.

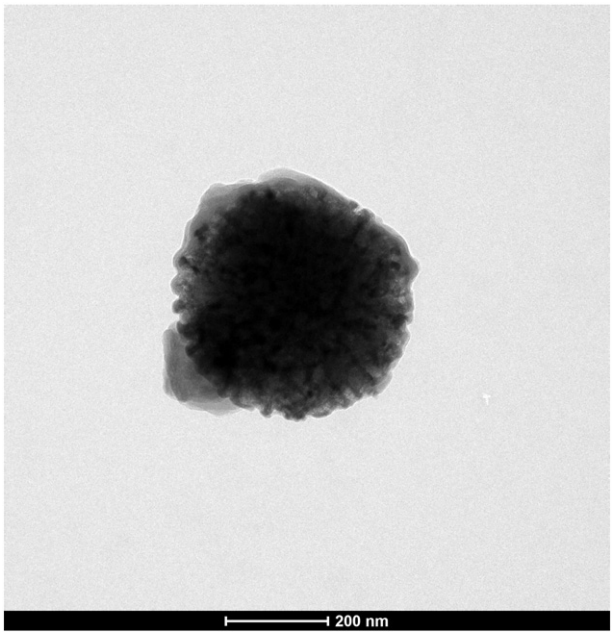

Fig. 14. TEM image of iron hydroxide particle.

the atomic percentage, the ratio of Ca/O is close to 1/2 (31.9/65.6), suggesting it was Ca $(OH)_2$.

Several spherical Si-bearing particles (ID: 23) with dark color were detected in Fig. 24, which had the size of 194 nm and 306 nm in diameter. These particles mainly consist of O (71.4%) and Si (15.4%), with a small amount of Na (2.9%), Mg (3.2%) and Al (3.9%). The atomic percentages suggested that these particles might be silicates.

Fig. 25 showed irregular Na, K-bearing particles (ID: 24). From the EDS analysis data, they mainly contained O (59.8%), Na (19.8%) and K (13.8%), with a small amount of Cl (2.6%), S (1.5%) and Zn (1.4%), suggesting they were oxides of Na and Mg.

Fe, Mn-bearing particles (ID: 25) with vague boundary were observed in Fig. 26. Their main components were O (48.8%), Fe (29.9%) and Mn (12.5%), suggesting they might be oxides of Fe and Mn.

5. Discussion

5.1. Comparison of the particle characteristics in the collected water samples

The ore-forming particles found in the deep groundwater samples have the following characteristics: These particles generally exist in the form of aggregates, with the size of a single particle ranging from 20 to 300 nm. These sizes of nanoscale particles are small enough to easily migrate along with the groundwater flow. The forms of the single particle are spherical, nearly spherical, elliptical, nearly polygonal and irregular, while the forms of the aggregates are irregular and chain-like assemblages. The shape of single particles with good crystallization may be more regular than the shape of aggregate particles that have also been seen in prior studies (Wei et al., 2013; Cao et al., 2009, 2010a,b). Fe mainly exists in the form of chain-like hematite and nearly rectangular iron hydroxide particles; Cu exists as irregular native copper and Cu oxide particles; and Zn-bearing particles often accompany Fe, Mn, Pb-bearing particles. Elliptical and irregular Zn, Mn oxide and spherical Zn, Pb sulfate are found. AgI particles and natural gold particles are found.

In the well water samples, particles of oxides and hydroxides of Fe with irregular or nearly spherical shape exist, and Mn, Cr oxide particles usually appear along with Fe-bearing particles. Cu_2O and CuO particles of irregular shape are found. Nearly spherical Zn oxide and irregular Pb oxide particles exist as well, which usually occur together and with Cu-bearing particles. The forms of the single particles are irregular, spherical and nearly rectangle, while the form of the aggregates is usually irregular.

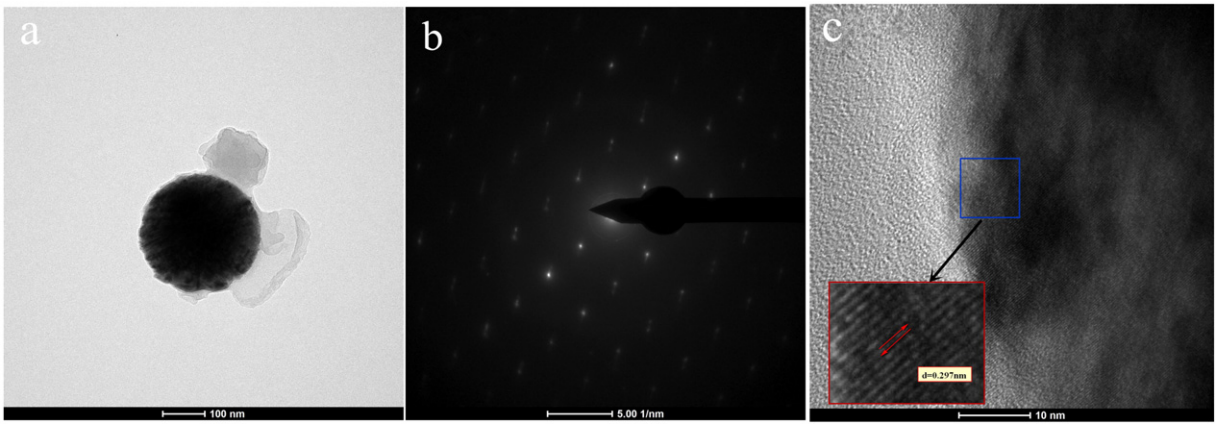

Fig. 13. Magnetite particle: a.TEM image, b. SAED image, c. HRTEM image.

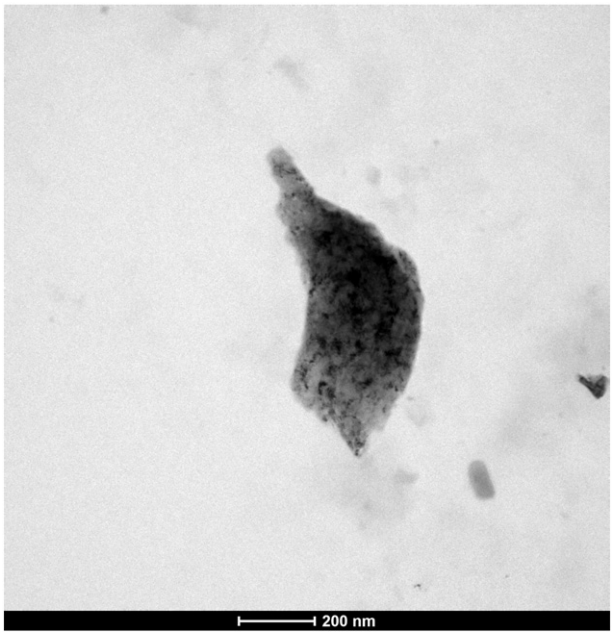

Fig. 15. TEM image of Fe, Mn, Cr-bearing particle.

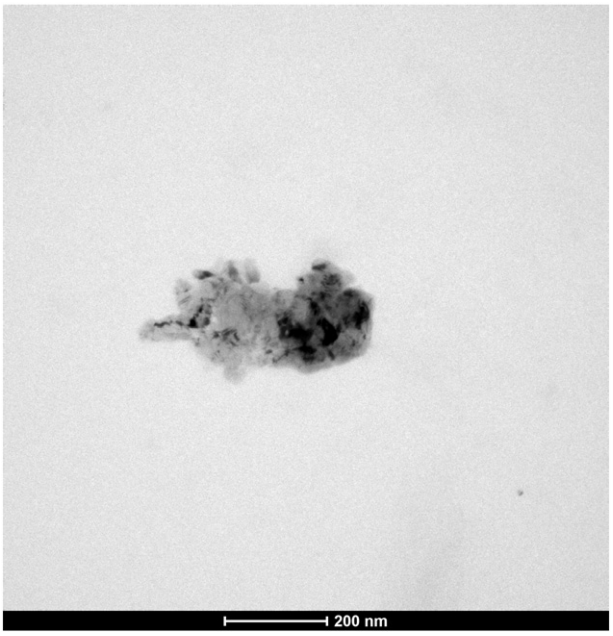

Fig. 17. TEM image of CuO particles.

Comparing the deep groundwater and well water particles, ore-forming metal particles, such as Fe, Cu, Pb and Zn-bearing particles were found in both types of water samples. Due to the oxygen-rich environment in the water, the occurrence state of these particles is mainly in the form of metal oxide. The elemental composition of these particles show that the well water samples present more obvious abnormities in the EDS data, for example, the elemental content of Cu, Zn and Pb are relatively higher than that in the deep groundwater samples. In addition, the ore-forming elements reveal some combination relationship, with some metal elements usually occurring together. Zn–Cu–Pb may be one combination, and Fe–Mn–Cr or Zn–Fe–Mn may be another one.

Based on the TEM analysis of the well water particles from the background area, the samples mainly contain particles of $CaCO_3$, $Ca(OH)_2$, oxygen-rich silicates, Na, K and Fe oxides. Some Zn and Cu particles exist, but the EDS patterns reveal that Zn and Cu abundances are low and near the background value, which means only minimal amounts of Zn and Cu were present. Therefore, even though a few Zn and Cu-bearing particles may exist, these samples are clearly from a background area with typical crustal material particles and are quite different from the ore bearing area. In addition, well water samples are similar to the deep groundwater samples, which can detect the ore-forming particles and exhibit high content of ore-forming elements, while the background waters can't. In addition, well water can be collected conveniently above ground. Thus these samples can be used to predict whether a deep mine exists or not. Compared with drilling and blasting, performing TEM experiments on the collected well water around the opencast mine is a simple method, to determine if there are particles with a high content of abnormal elements. Using this water sampling approach, if the elements determined in the water have some combination relationship that are not detected in the water collected in a non-ore area, then the wells where the water was sampled has a great possibility of having a deep mine around the wells.

5.2. The relationship between metal-bearing particles in well waters and the concealed ore body

Through a comprehensive correlation of the electron probe data of deep minerals (Li et al., 2014) and TEM analysis data of the well waters around the Dongshengmiao deposit, the following similarities can be observed.

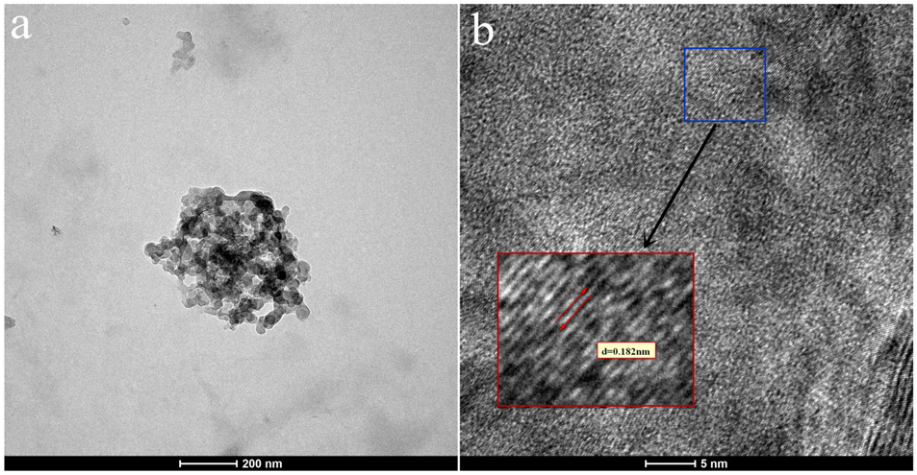

Fig. 16. Cu_2O particle: a.TEM image, b. HRTEM image.

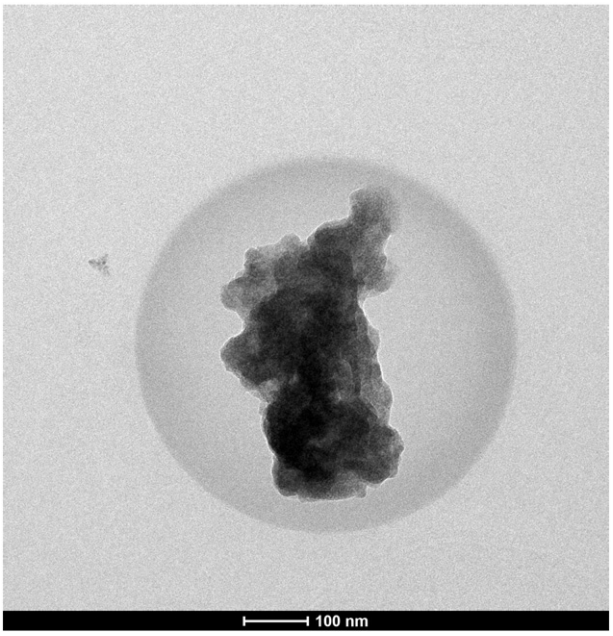

Fig. 18. TEM image of Zn, Cu oxide particles.

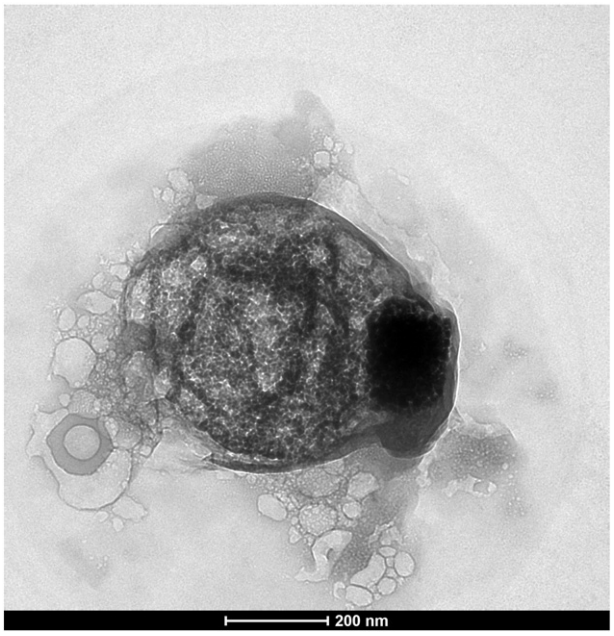

Fig. 20. TEM image of Pb oxide particles.

The electron probe data can further confirm that the deep ore body in the study area is primarily sulfide minerals, most of which are ferrous sulfide minerals, including pyrite, galena, sphalerite, pyrrhotite and a small amount of chalcopyrite. Sphalerite and chalcopyrite mainly grow with pyrite, and the latter is usually distributed around the pyrite. The TEM analysis data of the well water reveal that there are more Fe, Cu, Zn and Pb-bearing particles, of which Fe mainly exists as iron oxide and hydroxide; Cu exists as Cu_2O and CuO; Zn exists as zinc oxide like ZnO; and Pb also exists as oxide of Pb.

As previously discussed, oxidation or faulting caused some of the metal particles present in the well water samples to be in the form of oxides in high valence states. The majority of metal particles in the well waters exhibited similarities to the metal mineral composition of deep ore (Li et al., 2014). Furthermore, the combination relationship of Zn–Cu–Pb, Fe–Mn–Cr in well waters samples and Zn–Fe–Mn in deep groundwater is similar to the Fe–Cu–Zn combination of deep ore. Therefore, the well water particles and the minerals of the concealed ore body exhibit similar characteristics, and the ore-forming elements from the concealed ore bodies can be found in well water near the corresponding mining districts. Such results may further indicate that these ore-forming metal particles come from the concealed ore bodies and could be of great significance for prospecting.

5.3. The formation of ore-forming particles in groundwater

Regarding the formation of insoluble particles in concealed ore bodies, Tong et al. (1998) held the view that the particles may be distributed in the ore bodies and the surrounding rock during the process of

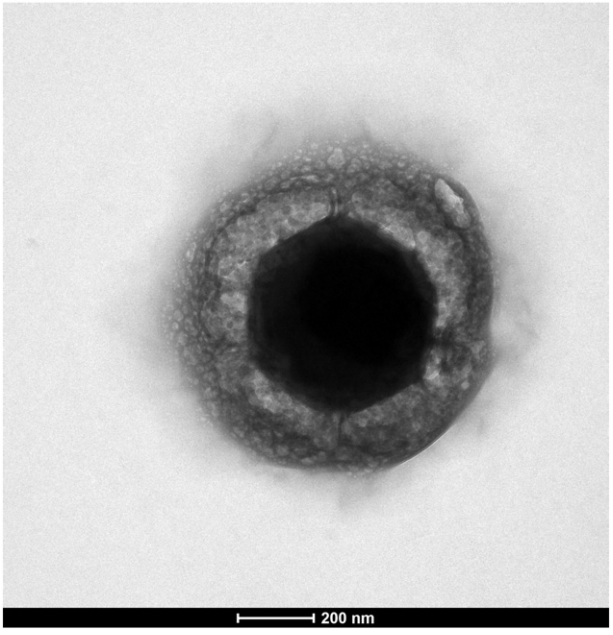

Fig. 19. TEM image of ZnO particle.

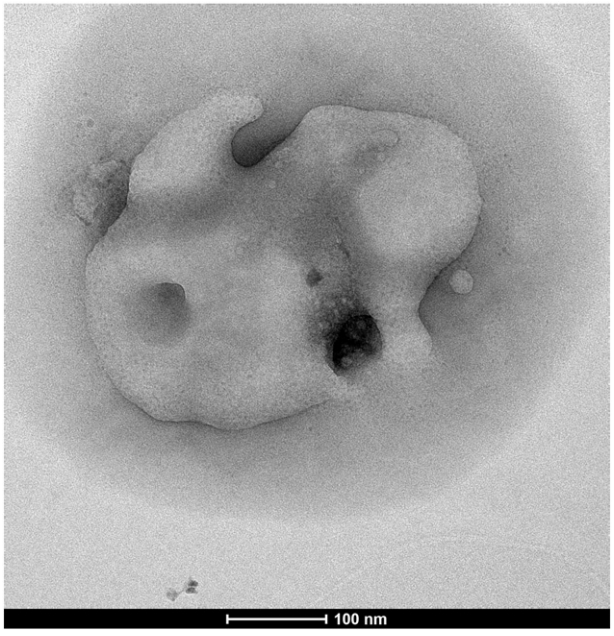

Fig. 21. TEM image of Zn, Pb, Cu oxide particles.

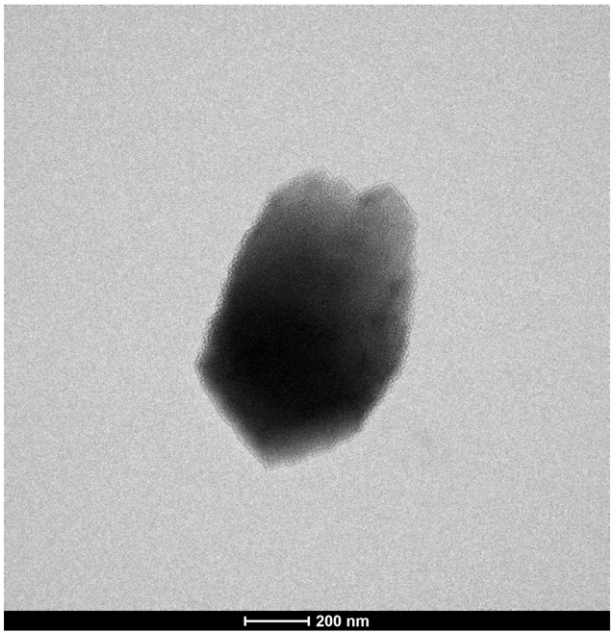

Fig. 22. TEM image of $CaCO_3$ particle.

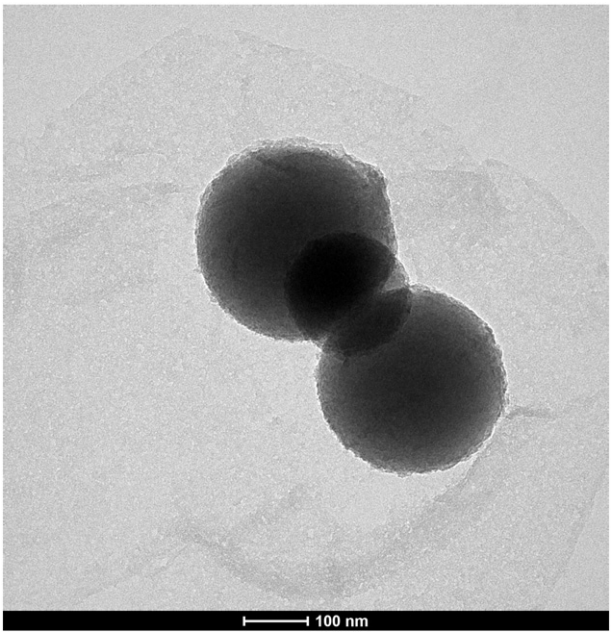

Fig. 24. TEM image of silicate particles.

mineralization. Cao et al. (2010a,b) indicated that particles mainly form after the metallogenic period and are primarily affected by faulting, oxidation and biological action. By combining the geological environment of the mining district, migration, and the characteristics and occurrence status of particles in the groundwater, the formation of these ore-forming particles can be hypothesized to have occurred in the following two ways. One way is faulting. The fracture is more developed in the mining area, and the Dongshengmiao mining area is located between regional faults F1 and F5 (see Fig. 1). Many small fractures are found in the mine as well. The process in the concealed ore bodies that converted material into particles with the help of the fracture was observed during the field study. Therefore, the existence of a fault promoted the formation of concealed ore body particles.

Simultaneously, due to the changes in the environmental conditions, such as temperature and pressure in the process of faulting, the nearby mineral composition may have undergone chemical reactions, including oxidation, which may transform the early formation of ore particles and raise the valence states of metal elements. The groundwater can remove some of the metal particles when it flows through the fissure of the fault mineralized belt.

Another mechanism is oxidation. The primary ore body is mainly composed of metal sulfides, such as pyrite, chalcopyrite, galena and sphalerite. In the tunnels of the mining area, except where the primary ore bodies are transformed by faulting, some veined pyrite was also found in the graphite schist and marble of the surrounding rock. However, the particles in the study are mainly in the form of high oxidation states like sulfates.

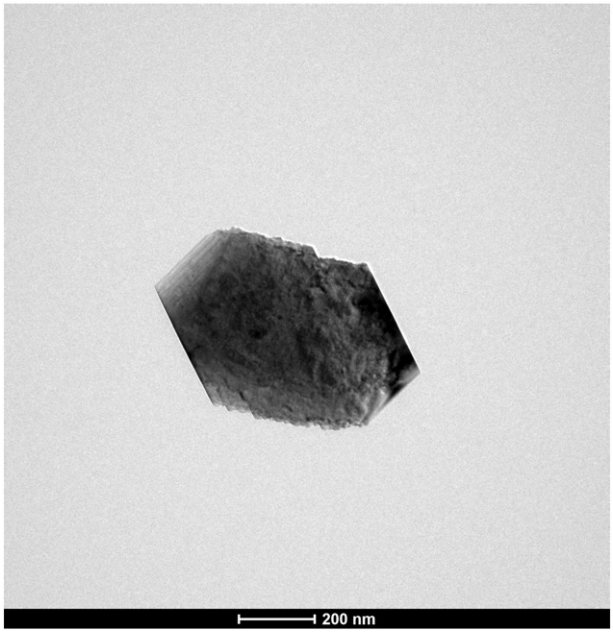

Fig. 23. TEM image of Ca $(OH)_2$ particle.

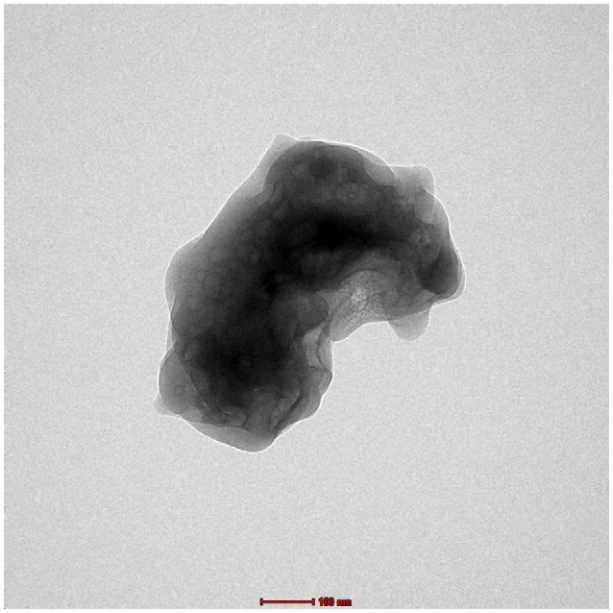

Fig. 25. TEM image of Na, Mg oxide particles.

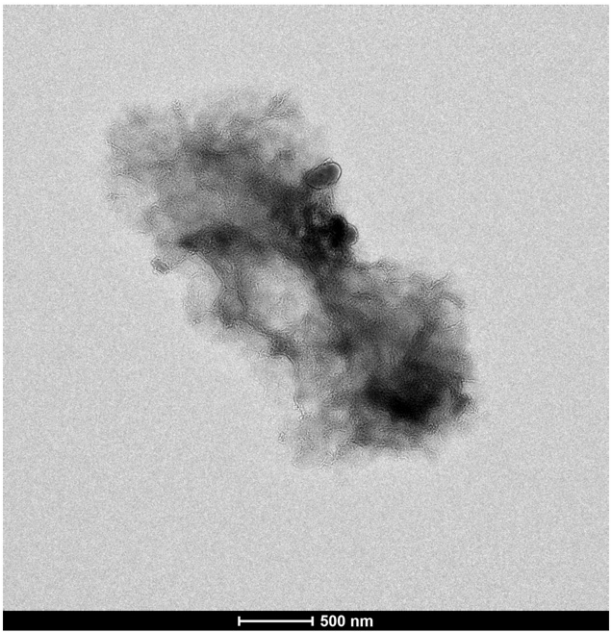

Fig. 26. TEM image of Fe, Mn oxide particles.

Under normal circumstances, the concealed ore bodies should be in reducing environments. The observed situation shows that abnormal-valence elements transformed from low valence states to high valence state such that the environment had to provide oxygen. One possibility is that when the fissure formed by faulting is connected with the surface, oxygen can constantly be transported from the surface through the fissure. The oxygen may result in the formation of sulfate and metal minerals during the process of oxidation of the metal sulfide. This oxidation is different from the oxidation of faulting. The former oxidation is the result of the fissure providing a channel for transporting oxygen. The latter is that of oxidation reaction occurring during the process of faulting. Some metal sulfides may be dissolved and released in the form of sulfate following oxidation, and then migrate in the groundwater.

Another possibility is that the rainy season usually occurs from June to September and provides water that infiltrates into the system. The bedrock fissure water is the dominant groundwater of the Dongshengmiao deposit, where the storage and the main migration channels of groundwater mainly rely on the fissure (Liu and Qian, 2012). Consequently, the oxygen-rich phreatic water can recharge the fissure water in the rainy season. The oxidized ore particles and oxygen can be carried by the phreatic water and then migrate to the underground.

Particles may be enriched during the period of drilling and blasting, however, ore-forming particles were found in the groundwater that were collected in or around the mine area, which were not detected only near the drilling or blasting area. Thus, these factors may have little influence on the creation of the observed ore-forming particles. Besides, the influence of drilling or blasting may weaken with groundwater flow and as time goes by.

5.4. The prospecting significance of groundwater particles

This paper is the first to use transmission electron microscopy (TEM) to study nano-scale groundwater particles in or around the ore district, and to analyze the morphology, size, aggregation state, structure, chemical composition and combination relationship of particles in the water samples. Compared with traditional methods, the proposed method can reflect more abundant metallogenic information. Finding metal particles in groundwater is an important discovery and may represent an innovative approach for concealed ore prospecting. To test whether the concealed ore bodies exist or not, the metal particles can be compared with the compositional relationships of observed ore bodies in the research area and particles in the research area can be compared with the particles from the background zones. The groundwater may have vertical and lateral migration (Dilinas et al., 2009). When the ore indicator particles are found in the groundwater, such as well water, we can delineate the abnormal area and then make a judgment on the general location of concealed ore bodies. By analyzing the geological background of the Dongshengmiao ore field, and the TEM data from well water samples, we can determine that there are more metal particles in the well water samples, and that these metal particles are relatively consistent with the composition of the indicator elements of the mining area.

Because the structure of the mining area is more fractured with both large and small fractures, the fault structure has close relationship with the mineralized zone. When the groundwater undergoes vertical migration, part of the metal particles may be carried when it flows through the fissure of the fractured mineralized belt. Therefore, if ore indicator particles are collected in such sampling sites, then the general location of concealed ore bodies can be estimated in accordance with the fault type and trend of this site. We can collect shallow groundwater samples along the faults that outcrop the surface, and analyze whether ore-forming particles exist. In another situation, the groundwater may undergo lateral migration when it flows in a horizontal direction. Slow flow velocity can provide an opportunity for leaching when it flows through the concealed ore body, as the metal particles may flow from deep groundwater to the well water, and the range of mineralized zone can be traced back in line with the flow direction and velocity of the groundwater.

This method can be combined with other geochemical or geophysical methods, which may verify the anomaly and improve the effectiveness and success rate of the prospecting. By comparing the combination and characteristic of the particles with the features of the ore-forming element, we can provide a weight of evidence argument as to the existence of the concealed ore bodies and estimate the location of deep ore bodies, which may improve the success rate of drilling prospecting.

6. Conclusions

After collecting the groundwater samples in or near the ore district, transmission electron microscopy (TEM) was used to analyze the morphology, size, component and structure of the particles in the water samples. By combining the known characteristics of the mining area and the particles in the samples, we can draw the following conclusions through comparison and analysis.

I. Particles in water samples mainly exist in the form of polymeride, and the size of a single particle ranges from 20 to 300 nm. The shapes of the particles are varied, including nearly spherical, elliptical, nearly polygonal, irregular and so on.

II. From the TEM analysis, the ore-forming metal particles, such as Fe, Cu, Pb and Zn-bearing particles are found in both well water and deep groundwater. Well water samples show more obvious abnormality in the EDS data, which can detect the ore-forming particles and reveal a high content of ore-forming elements in contrast to the background waters. The features, elemental ratios and chemical components in well water samples are consistent with deep ore bodies, which may indicate that they come from concealed ore bodies. These features can be used to predict whether a deep ore body exists.

III. Faulting and oxidation are major mechanisms for the formation of ore-forming particles. These particles provide information regarding the concealed ore body. By examining the characteristics of groundwater particles and their relationship with the concealed ore body, a new method for groundwater particle geochemical prospecting can be proposed.

Acknowledgments

This project was supported by the National Natural Science Foundation of China (grant numbers: 41030425, 41473040). We wish to thank Wang Qingli and Li Yuqing of the Instrument Analysis Center of the Yangzhou University for the help with microscopic analysis. We are grateful to the two anonymous reviewers and the editor Prof. Changjiang Li for providing valuable comments and suggestions, which have greatly improved the quality of the paper.

References

Antropova, L.V., Goldberg, I.S., Voroshilov, N.A., Ryss, J.S., 1992. New methods of regional exploration for blind mineralization: application in the USSR. J. Geochem. Explor. 43 (2), 157–166.

Arne, D.C., Stott, J.E., Waldron, H.M., 1999. Biogeochemistry of the Ballarat East Goldfield, Victoria, Australia. J. Geochem. Explor. 67 (1), 1–14.

Cameron, E.M., Hamilton, S.M., Leybourne, M.I., 2004. Finding deeply buried deposits using geochemistry. Geochem. Explor. Environ. Anal. 4 (1), 7–32.

Cao, J.J., Hu, R.Z., Liang, Z.R., Peng, Z.L., 2009. TEM observation of geogas-carried particles from the Changkeng concealed gold deposit, Guangdong Province, South China. J. Geochem. Explor. 101 (3), 247–253.

Cao, J.J., Hu, X.Y., Jiang, Z.T., Li, H.W., Zou, H.Z., 2010a. Simulation of adsorption of gold nanoparticles carried by gas ascending from the Earth's interior in alluvial cover of the middle-lower reaches of the Yangtze River. Geofluids 10 (3), 438–446.

Cao, J.J., Liu, C., Xiong, Z.H., Qin, T.R., 2010b. Particles carried by ascending gas flow at the Tongchanghe copper mine, Guizhou Province. Sci. China Earth Sci. 53 (11), 1647–1654.

Cao, J.J., Li, Y.K., Jiang, T., Hu, G., 2015. Sulfur-containing particles emitted by concealed sulfide ore deposits: an unknown source of sulfur-containing particles in the atmosphere. Atmos. Chem. Phys. 15 (12), 6959–6969.

Chen, X.F., Peng, R.M., 2008. Analysis on the geological structural factors leading to the Dongshengmiao super-large deposit. Contrib. Geol. Miner. Resour. Res. 23 (3), 182–186 (in Chinese with English abstract).

Cidu, R., Fanfani, L., Shand, P., Edmunds, P.S., Vandack, L., Gijbels, R., 1995. Hydrogeochemical exploration for gold in the Osilo area, Sardinia, Italy. Appl. Geochem. 10 (5), 517–529.

Clark, J.R., Meier, A.L., Riddle, G., 1990. Enzyme leaching of surficial geochemical samples for detecting hydromorphic trace-element anomalies associated with precious-metal mineralized bedrock buried beneath glacial overburden in northern Minnesota. Proceedings of the Gold'90 Symposium-Gold'90, pp. 189–207.

Cole, M.M., 1971. The importance of environment in biogeographical/geobotanical and biogeochemical investigations. J. South. Afr. Inst. Min. Metall. 11, 414–425.

Costantini, E.A.C., Lessovaia, C., Vodyanitskii, Y., 2006. Using the analysis of iron and iron oxides in paleosols (TEM, geochemistry and iron forms) for the assessment of present and past pedogenesis. Quat. Int. 156, 200–211.

Dilinas, J., Jurevicius, A., Karveliene, D., 2009. Migration forms of main chemical elements in the groundwater of the Quaternary deposits of Lithuania. Baltica 22 (2), 123–132.

Eppinger, R.G., Fey, D.L., Giles, S.A., Kelly, K.D., Smith, S.M., 2012. An exploration hydrogeochemical study at the giant Pebble porphyry Cu–Au–Mo deposit, Alaska, USA, using high resolution ICP-MS. Geochem. Explor. Environ. Anal. 12 (3), 211–226.

Erg, K., 2005. Groundwater Sulphate Content Changes in Estonian Underground Oil Shale Mines. Tallinn University of Technology Press.

Hill, S.M., Hill, L.J., 2003. Some important plant characteristics and assay overviews for biogeochemical surveys in western New SouthWales. Advances in Regolith. CRC LEME, pp. 187–192.

Hu, G., Cao, J.J., Hopke, P.K., Holub, R.F., 2015. Study of carbon-bearing particles in ascending geogas flows in the Dongshengmiao polymetallic pyrite deposit, Inner Mongolia, China. Resour. Geol. 65 (1), 13–26.

Huff, L.C., 1948. A sensitive field test for heavy metals in water. Econ. Geol. 43 (8), 675–684.

Jiang, X.Q., 1993. The geological characteristics of Dongshengmiao pyrite-polymetallic sulfide deposit, Inner Mongolia. Acta Geosci. Sin. 14 (Z1), 103–115 (in Chinese with English abstract).

Johanna, L.P., Jorg, E., Martin, Z., 2011. Geogas transport in fractured hard rock—correlations with mining seismicity at 3.54 km depth, TauTona gold mine, South Africa. Appl. Geochem. 26 (12), 2134–2146.

Kelley, D.L., Hall, G.E.M., Graham, C.L., Hamilton, I.A., Mcewen, R.M., 2003. The use of partial extraction geochemistry for copper exploration in northern Chile. Geochem. Explor. Environ. Anal. 3 (1), 85–104.

Kumar, M., Ramanathan, A.L., Rao, M.S., Kumar, B., 2006. Identification and evaluation of hydrogeochemical processes in the groundwater environment of Delhi, India. Environ. Geol. 50 (7), 1025–1039.

Lakshmanan, E., Kannan, R., Kumar, M.S., 2003. Major ion chemistry and identification of hydrogeochemical processes of ground water in a part of Kancheepuram district, Tamil Nadu, India. Environ. Geosci. 10 (4), 157–166.

Li, Y.K., Cao, J.J., Wu, Z.Q., Dai, D.L., Lin, Z.X., 2014. The research on deep ore composition of Dongshengmiao mining area, Inner Mongolia. Met. Miner. 10, 110–113 (in Chinese with English abstract).

Liu, Y., Qian, J.Q., 2012. The geological characteristics and prospecting of Dongshengmiao ore deposit, Inner Mongolia. Gansu Sci. Technol. 28 (9), 44–46 (in Chinese with English abstract).

Mann, A.W., Birrell, R.D., Mann, A.T., Humphreys, D.B., Perdrix, J.L., 1998. Application of the mobile metal ion technique to routine geochemical exploration. J. Geochem. Explor. 61 (1), 87–102.

McHugh, J.B., 1988. Concentration of gold in natural waters. J. Geochem. Explor. 30 (1), 85–94.

Miller, W.R., Ficklin, W.H., Learned, R.E., 1982. Hydrogeochemical prospecting for porphyry copper deposits in the tropical-marine climate of Puerto Rico. J. Geochem. Explor. 16 (3), 217–233.

Mohammadzadeh, M.J., Chary, D.V., 2005. A tool to groundwater prospecting in granitic terrain of Hyderabad Region AP, India. J. Appl. Sci. Res. 1 (1), 85–89.

Nikic, Z., Kovacevic, J., Papic, P., 2008. Uranium in the groundwater of Permo-Triassic aquifers of the Visok Region, Stara Planina, Eastern Serbia. Water Air Soil Pollut. 192 (1–4), 47–58.

Peng, R.M., Zhai, Y.S., Han, X.F., Wang, J.P., Qin, J.W., 2007. Magmatic hydrothermal overprinting in the Mesoproterozoic Dongshengmiao deposit, Inner Mongolia: geological and fluid inclusion evidences. Acta Petrol. Sin. 23 (1), 145–152.

Randrianantoandro, N., Mercier, A.M., Hervieu, M., Greneche, J.M., 2001. Direct phase transformation from hematite to maghemite during high energy ball milling. Mater. Lett. 47 (3), 150–158.

Rani, A., Mehra, R., Duggal, V., Balaram, V., 2013. Analysis of uranium concentration in drinking water samples using ICPMS. Health Phys. 104 (3), 251–255.

Ryss, Y.S., Goldberg, I.S., 1973. The partial extraction of metals (CHIM) method in mineral exploration. Method and Technique, ONTI, VITR, Leningrad 84, pp. 5–19.

Shvartsev, S.L., 2009. Hydrogeochemical prospecting for blind ores in permafrost. Int. Geol. Rev. 14 (10), 1037–1043.

Singha, L., Singh, L., Kher, S., 2003. A comparison of fission track and laser fluorometry techniques for uranium analysis in water samples. Radiat. Meas. 36 (1), 517–519.

Song, M.C., Wan, G.P., Cao, C.G., He, C.Y., 2012. Geophysical–geological interpretation and deep-seated gold deposit prospecting in Sanshandong-Jiaojia Area,Eastern Shandong Province, China. Acta Geol. Sin. (Engl. Ed.) 86 (3), 640–652.

Taufen, P.M., 1997. Ground waters and surface waters in exploration geochemical surveys. Explor. Geochem. 97, 271–284.

Tong, C.H., Li, J.C., Ge, L.Q., Yang, F.G., 1998. Experimental observation of the nano-scale particles in geogas matters and its geological significance. Sci. China Ser. D Earth Sci. 41 (3), 325–329.

Varentsov, I.M., Sokolova, E.Y., 2003. Diagnostics and suppression of auroral distortions in the transfer operators of the electromagnetic field in the BEAR experiment. Izv. Phys. Solid Earth 39, 283–307.

Varentsov, I.M., Kulikov, V.A., Yakovlev, A.G., Yakovlev, D.V., 2013. Possibilities of magnetotelluric methods in geophysical exploration for ore minerals. Phys. Solid Earth 49 (3), 309–328.

Wang, X.Q., 2003. Delineation of geochemical blocks for undiscovered large ore deposits using deep-penetrating methods in alluvial terrains of eastern China. J. Geochem. Explor. 77 (1), 15–24.

Wang, X.Q., Cheng, Z., Lu, Y., 1997. Nanoscale metals in earthgas and mobile forms of metals in overburden in wide-spaced regional exploration for giant deposits in overburden terrain. J. Geochem. Explor. 58 (1), 63–72.

Wang, X.Q., Xie, X.J., Cheng, Z.Z., Liu, D.W., 1999. Delineation of regional geochemical anomalies penetrating through thick cover in concealed terrains — a case history from the Olympic dam deposit, Australia. J. Geochem. Explor. 66 (1), 85–97.

Wang, D., Yan, F.Y., Chen, J.J., 2013. Application of geophysical and geochemical exploration results in prospecting prediction:taking Pangjiagou-Xiajinbaogou Au–Ag polymetallic ore in Hebei Chengde as an example. Adv. Mater. Res. 807, 2192–2196.

Wei, X.J., Cao, J.J., Holub, R.F., Hopke, P.K., Zhao, S.J., 2013. TEM study of geogas-transported nanoparticles from the Fankou lead–zinc deposit, Guangdong Province, South China. J. Geochem. Explor. 128, 124–135.

Ye, R., Wang, X.Q., Zhang, B.M., 2014. A microscopic and nanoscale understanding of the formation of gold geochemical provinces. Acta Geol. Sin. (Engl. Ed.) 88 (3), 995–1003.